ACS APPLIED MATERIALS & INTERFACES

Research Article

www.acsami.org

Highly Improved Efficiency of Deep-Blue Fluorescent Polymer Light-Emitting Device Based on a Novel Hole Interface Modifier with 1,3,5-Triazine Core

Lianpeng Xia,[†] Yuyuan Xue,[†,‡] Kang Xiong,[†] Chaosheng Cai,[†] Zuosheng Peng,[†] Ying Wu,[‡] Yuan Li,*[,‡] Jingsheng Miao,[§] Dongcheng Chen,[§] Zhanhao Hu,[§] Jianbin Wang,[§] Xiaobin Peng,[§] Yueqi Mo,[§] and Lintao Hou*[,†]

[†]Siyuan Laboratory, Department of Physics, Jinan University, Guangzhou 510632, P.R. China

[‡]School of Chemistry and Chemical Engineering, South China University of Technology, Guangzhou 510640, P.R. China

[§]Institute of Polymer Optoelectronic Materials and Devices, State Key Laboratory of Luminescent Materials and Devices, South China University of Technology, Guangzhou 510640, P.R. China

Supporting Information

ABSTRACT: We present an investigation of deep-blue fluorescent polymer light-emitting diodes (PLEDs) with a novel functional 1,3,5-triazine core material (HQTZ) sandwiched between poly(3,4-ethylene dioxythiophene):poly-(styrene sulfonic acid) layer and poly(vinylcarbazole) layer as a hole injection layer (HIL) without interface intermixing. Ultraviolet photoemission spectroscopy and Kelvin probe measurements were carried out to determine the change of anode work function influenced by the HQTZ modifier. The thin HQTZ layer can efficiently maximize the charge injection from anode to blue emitter and simultaneously enhance the hole mobility of HILs. The deep-blue device performance is remarkably improved with the maximum luminous efficiency of 4.50 cd/A enhanced by 80% and the maximum quantum efficiency of 4.93%, which is 1.8-fold higher than that of the conventional device without HQTZ layer, including a lower turn-on voltage of 3.7 V and comparable Commission Internationale de L'Eclairage coordinates of (0.16, 0.09). It is the highest efficiency ever reported to date for solution-processed deep-blue PLEDs based on the device structure of ITO/HILs/poly(9,9-dialkoxyphenyl-2,7-silafluorene)/CsF/AL. The results indicate that HQTZ based on 1,3,5-triazine core can be a promising candidate of interfacial materials for deep-blue fluorescent PLEDs.

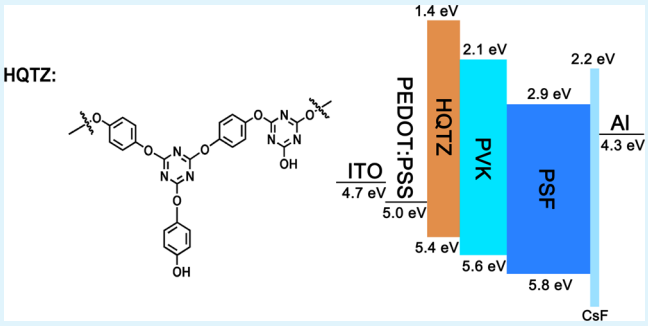

KEYWORDS: *1,3,5-triazine core, deep-blue, fluorescent polymer light-emitting diodes, hole injection layer, charge balance*

INTRODUCTION

Polymer light-emitting diodes (PLEDs) have attracted greatly scientific and industrial attention because of their potential applications in large-area solid-state lighting and thin film transistor displays.[1−4] However, the blue-light fluorescent PLEDs have not been able to get the considerable efficiency compared with the green and red fluorescent PLEDs.[5] It is well-known that highly efficient blue-light fluorescent PLED is one of the major challenges to further accelerate commercialization of full color display and lighting source applications.[6−9] According to the National Television Standards Committee (NTSC), standard blue light is required to be at Commission Internationale de L'Eclairage (CIE) coordinates of (0.14, 0.08).[10] The preferred CIE coordinates are in the deep-blue area, implying that only a very wide energy band gap would lead to deep-blue emitting. Polymeric deep-blue emitters have drawn much attention as deep-blue emitters in PLEDs due to their large energy band gap, good thermal stability, and high photoluminescence quantum efficiency as well as simple and cheap film-forming ability for the large-scale commercial production of the devices. The highest efficiencies ever achieved among the best deep-blue PLEDs performances are 7.28% and 4.88 cd/A, respectively, with a maximum luminance of 14700 cd/cm^2 and CIE coordinates of (0.16, 0.07) based on polyspirofluorene with dual hole-transporting moieties.[11] However, besides the ingenious molecular design of the polymeric blue emitters, the corresponding solution-processing hole injection or electron injection materials, which match to polymeric blue emitters without interface mixing, are rarely synthesized and investigated.

Generally, the effective electron injection from cathode is feasible to achieve due to the facile matching between the

Received: February 6, 2015
Accepted: September 30, 2015
Published: September 30, 2015

DOI: 10.1021/acsami.5b06068
ACS Appl. Mater. Interfaces 2015, 7, 26405−26413

lowest unoccupied molecular orbital (LUMO) energy level of blue emitters and the low-work-function alkaline earth metals or alkali salts.[12] Subsequently, the most important factor restricting the blue-light device performance is the limited hole injection from anode to blue emitter, which possesses very deep highest occupied molecular orbital (HOMO) energy level.[3,13] For solving this problem, various hole injection layers (HILs) are inserted between tin-doped indium oxide (ITO) and blue emitter such as poly(3,4-ethylene dioxythiophene):poly(styrene sulfonic acid) (PEDOT:PSS)/poly(vinylcarbazole) (PVK),[14−16] MoO_3,[17] etc. However, there still exists a large injection barrier to approach ohmic contact.[18] The work function of ITO is only about 4.7 eV, while the HOMO energy levels of the blue emitters are typically located from 5.5−6.3 eV, leading to the discontinuous laminated ohmic contact between ITO and deep-blue emitter with injection barrier higher than 0.3 eV.[2,13,19] Although multiple HILs are applied to match the energy level of ITO and deep-blue emitters to improve the hole injection, the big HOMO energy level gap among HILs, for example, PEDOT:PSS and PVK, is still difficult to overcome to maximize the performance of deep-blue emitters.[20]

The electron-deficient 1,3,5-triazine derivatives have been widely used as electron transport materials,[21−23] hole transport materials,[24] and bipolar transport materials.[25] However, there is no report on hole injection materials based on electron-deficient 1,3,5-triazine and electron-rich compounds such as phenol and its derivatives with preferred solution processing ability. In this paper, we propose and design a novel hole interface modifier material based on polymerization of hydroquinone and 2,4,6-trichloro-1,3,5-triazine (HQTZ). The resulted polymer contains phenol group as terminal group. Our concept is confirmed by the systematic study using HQTZ as HIL in a classical deep-blue poly(9,9-dialkoxyphenyl-2,7-silafluorene) (PSF) fluorescent PLED. PSF is a promising deep-blue fluorescent light-emitting polymer with good CIE (0.16, 0.08) and comparable high quantum efficiency (QE) of 2.02% when PEDOT:PSS/PVK were used as multiple HILs.[14] The HOMO energy level of PSF is ∼5.8 eV, which is much higher than the work function of ITO anode (∼4.7 eV). Thus, it is essential to sandwich new intermediate HIL between PEDOT:PSS and PVK for further enhancing deep-blue PSF device performance. We found that HQTZ is excellently compatible with PEDOT:PSS and PVK and can further enhance the hole injection from ITO anode to PSF emitter and hole transport of multiple HILs. The deep-blue device performance is greatly improved by introducing HQTZ between PEDOT:PSS and PVK. To the best of our knowledge, this is the first report using HQTZ with 1,3,5-triazine core and phenol terminal group as HIL in deep-blue fluorescent PLEDs. The results indicate that with the development of more and more deep-blue emitters with ideal CIE coordinates (CIE_y < 0.1), the judicious molecular design of hole injection materials will furnish the desired blue pixel for future flat-panel displays and lighting sources.

EXPERIMENTAL SECTION

Preparation of HQTZ. The synthesis route of HQTZ is shown in Scheme 1. Hydroquinone (1.8 g, 16 mmol) was dissolved in a solution of aqueous sodium hydroxide solution (0.65 g, 16 mmol, in 30 mL of distilled water). Cyanuric chloride (1.0 g, 5.4 mmol) in acetone (10 mL) was added dropwise in 1 h. The reaction mixture was stirred at room temperature for 5 h. After the methanol was removed under reduced pressure, the residue was filtered by using a sintered-glass

Scheme 1. Synthesis Route of HQTZ

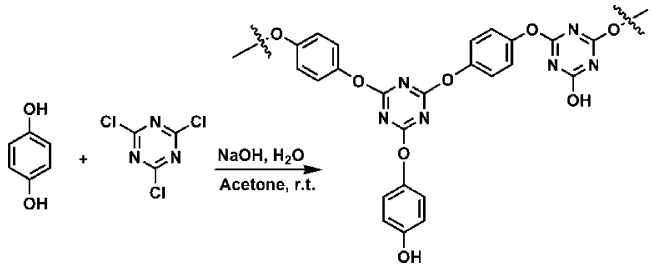

funnel and purified by washing with water and methanol. The filter cake dried under vacuum to yield a brown solid without any other purification process, and the yield was as high as 73%.

Cyclic voltammetry (CV) test was conducted with platinum electrodes at a scan rate of 100 mV/s against Hg/Hg_2Cl_2 reference electrode using ferrocene as internal standard in dry dichloromethane containing 0.1 M tetra-*n*-butylammonium hexafluorophosphate (nBu_4NPF_6) as a supporting electrolyte. ^1H NMR and ^{13}C HMR of HQTZ were recorded with 15 mg of sample dissolved in 0.5 mL of deuterated dimethyl sulfoxide (d_6-DMSO) using DRX-400 spectrometer (Bruker Co., Ettlingen, Germany). Electrospray ionization (ESI) mass spectrometry was recorded by Bruker-Esquire-3000. Matrix-assisted laser desorption/ionization time-of-flight (MALDI-TOF) mass spectrum was recorded on a Bruker Autoflex instrument using 1,8,9-anthracene triol as a matrix with the type of negative ion mode. The thermal stability of HQTZ was investigated by thermogravimetric analysis (STA449C, Netzsch). The optimum geometry and electron-state-density distribution of the HOMO and LUMO of the unimer were investigated by performing density functional theory (DFT) calculations at the B3LYP/6-31G (D) level using Gaussian 09 program suite. The solubility of HQTZ was tested carefully, and it showed moderate solubility of 15 g L^{-1} in DMSO to avoid mixing with the PEDOT:PSS layer as HQTZ was not soluble in water. HQTZ was not soluble in common organic solvents such as acetone, dichloromethane, and toluene.

Device Fabrication and Characterization. PSF[14] and PVK (Alfa) were dissolved in o-xylene with the concentration of 10 g L^{-1} and chlorobenzene with concentration of 15 g L^{-1}, respectively. All solutions were stirred for overnight before use. ITO substrates with a sheet resistance <10 Ω/sq were cleaned by a series of ultrasonication treatments in acetone, deionized water, and isopropyl alcohol. A 40 nm-thick PEDOT:PSS (Bayer Baytron P 4083) layer was spin-coated on the precleaned and O_2-plasma-treated ITO and baked at 120 °C for 20 min to remove residual water. HQTZ layers with different thicknesses of 10, 20, and 30 nm, were spin-coated on top of 40 nm-thick PEDOT:PSS layer. A 35 nm-thick PVK layer was spin-coated on 40 nm-thick PEDOT:PSS layer or HQTZ layer (10, 20, and 30 nm). For comparison, a 20 nm-thick HQTZ layer was directly spin-coated onto ITO substrates. A 75 nm-thick PSF layer was spin-coated on top of these HILs. Except the PEDOT:PSS layer, all the fabrication processes were carried out in a nitrogen-circulated glovebox. Finally, top electrodes of 1 nm cesium-fluoride (CsF) and 100 nm Al were evaporated in sequence at a pressure of 3×10^{-4} Pa. The thickness of the evaporated CsF and Al was monitored by a quartz crystal thickness/ratio monitor (STM-100/MF, Sycon). The thickness of relatively thick films was determined by a surface profiler (XP-2, Ambios). The active emission area of the devices is 0.14 cm^2.

The current density−luminance−voltage (*J*−*L*−*V*) characteristics were measured by a Keithley 2400 source measurement unit and a calibrated silicon photodiode. The luminance (*L*) and the luminance efficiency (*LE*) were calibrated by a spectrophotometer (SpectraScan PR-705, Photo Research). The quantum efficiency (*QE*) was amended by measuring the total light output in all direction in an integrating sphere (ISO-080, Labsphere). The electroluminescence (*EL*) spectra were collected via an optics photometer (USB4000, Ocean Optics). The photoluminescence (*PL*) intensities were measured by fluorescence spectrometer (RF-5301PC, Shimadzu). Time-resolved

DOI: 10.1021/acsami.5b06068
ACS Appl. Mater. Interfaces 2015, 7, 26405−26413

transient *PL* spectra were measured by spectrophotometer (FLS9200, Edinburgh). The photovoltaic measurements were carried out under an illumination of AM 1.5G solar simulator with the intensity of 100 mW/cm^2 (Sun 2000 Solar Simulator, Abet Technologies). The kinetic energy and work function of different HILs-modified ITO were measured by ultraviolet photoemission spectroscopy (ESCALAB 250, Thermo-VG Scientific) and scanning Kelvin probe force microscopy (SKP5050, Cross-Tech). The morphology and roughness of films were measured by atomic force microscope (AFM) (CSPM5500, Being Nano). The cross-section images were measured by scanning electron microscope (SEM) with an acceleration voltage of 15 kV (ULTRA55, Zeiss).

RESULTS AND DISCUSSION

Figure 1, panels a, b, and c present the experimental device architecture and schematic energy diagram of deep-blue

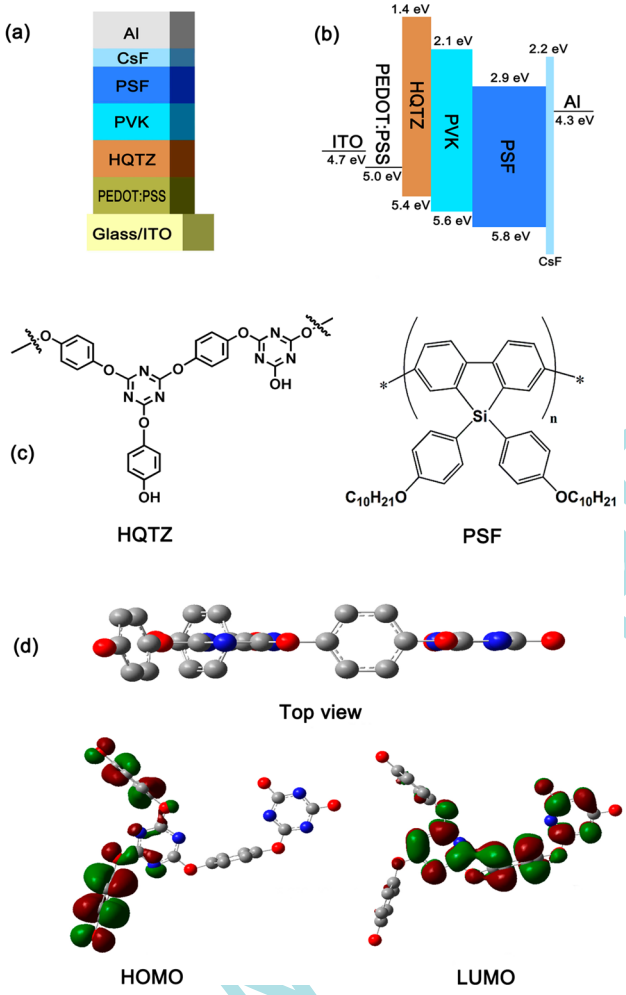

Figure 1. (a) Device architecture and (b) schematic energy diagram of deep-blue fluorescent PLEDs (**P1**) using HQTZ as an intermediate HIL. (c) The molecular structures of HQTZ and PSF. (d) DFT-optimized geometries and charge-density iso-surfaces for the HOMO and LUMO energy levels of HQTZ unimer.

fluorescent PLEDs **P1** (ITO/PEDOT:PSS/HQTZ(10, 20, or 30 nm)/PVK/PSF/CsF/Al) with HQTZ as an intermediate HIL, and the molecular structures of HQTZ and PSF. For comparison, device **P2** without HQTZ (ITO/PEDOT:PSS/PVK/PSF/CsF/Al), device **P3** without PEDOT:PSS/HQTZ (ITO/PVK/PSF/CsF/Al), and device **P4** without PEDOT:PSS (ITO/HQTZ(20 nm)/PVK/PSF/CsF/Al) were also fabricated as the control devices. As shown in Figure 1, panel d, the π-electrons are spread over the two phenol units at HOMO (energy level: −6.08 eV), while concentrated at the triazine unit at LUMO (energy level: −0.73 eV), indicating strong electron-donating ability of phenol and electron-accepting ability of triazine. The bipolar transport properties observed in the calculated HOMO and LUMO iso-surfaces suggest that HQTZ should be an efficient and versatile material for the applications in PLEDs.

To study the chemical structure of HQTZ, ^{1}H NMR, ^{13}C NMR, ESI, and MALDI-TOF mass spectrometer of HQTZ were conducted, and the results are shown in Figures S1−S4. The complex proton signals between 6.5 and 7.5 ppm in ^{1}H NMR spectrum are attributed to the phenyl groups in HQTZ, and ESI mass shows HQTZ is a mixture containing several low molecular weight oligomers. ^{13}C NMR spectrum also confirms its complex structure as it shows a series of signals in aromatic region. Although the structure is complex, the phenol structure is the main part in HQTZ. MALDI-TOF mass spectrum shows the fragment ion peaks of HQTZ, which are distributed in five different molecular weight ranges. Interestingly, the space between the two adjacent areas is about 200 Da, which is the molecular weight of the unit containing a benzene ring and a triazine building block. The gap of the adjacent fragment ion peaks is 16 Da. The cleavage of ether bond is proved with the loss of an oxygen atom. At the same time, there are a few doubly charged ions, indicating that the molecular weight of HQTZ is larger than the value of the fragment ion peaks. The color of HQTZ solution will change after several days, which means it is unstable in air. This result further confirms the structure we proposed previously. It also contributes its unexpected hole transport capability. The electrochemical property of HQTZ shows oxidation potential (E_{ox}) at 1.01 V (see Figure 2a), which is used to estimate a HOMO energy level of −5.41 eV according to the empirical formula $E_{HOMO} = -(E_{ox} + 4.4)$ (eV).[14] For comparison, the electrochemical property of PVK shows E_{ox} at 1.18 V, and a HOMO energy level of −5.58 eV is estimated. The HOMO energy level difference of ∼0.2 eV indicates that HQTZ is excellently compatible with PVK and can form step-by-step hole injection. It can be predicted that HQTZ can also be used to other deep-blue emitters as HIL, such as spiro-polyfluorene (sPF),[11] oligofluorenes (T1),[26] poly(9,9-dioctylfluorene) (PFO-ETM),[27] poly(9,9-di-n-octylfluorene-2,7-diyl) (PFO-TFP),[28] poly(3,6-(9,9-dihexyl)silafluorene) (PSiF),[29] and 9,9-dioctyl-fluorene (PSiC8OF0),[30] etc., due to the well-matched HOMO energy level with that of deep-blue emitters, as shown in Figure S5. This illustrates that HQTZ can be a promising hole injection material for deep-blue PLEDs. To determine the LUMO energy level, we combine the oxidation potential in CV with the optical energy band gap resulting from the absorption edge (309 nm) in an absorption spectrum (see Figure 2b). It can be used to estimate the LUMO energy level of −1.40 eV. As shown in Figure S6, the thermal decomposition temperature of 5% weight loss is around 192 °C in air atmosphere, which is adequate for its application in PLEDs and other optoelectronic devices.

Figure 3 presents the *J*−*V*, *L*−*V*, *LE*−*V*, and *QE*−*V* characteristics of deep-blue fluorescent PLEDs with/without (w/o) the HQTZ HIL. Compared with the control devices, device **P1** with a 20 nm-thick HQTZ layer shows the enhanced luminance and *EL* efficiency in conjunction with the lowest leaking current in the low voltage. A maximum *LE* of 4.50 cd/A

DOI: 10.1021/acsami.5b06068
ACS Appl. Mater. Interfaces 2015, 7, 26405−26413

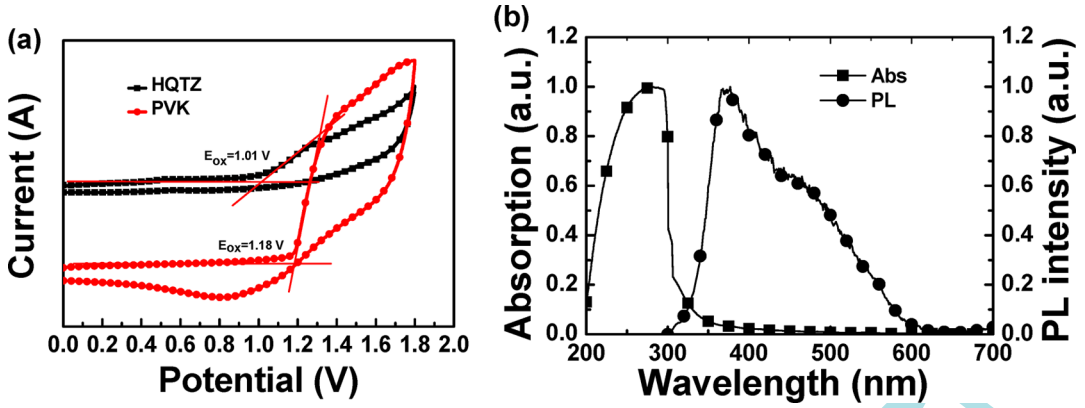

Figure 2. (a) Cyclic voltammograms of HQTZ and PVK in dry CH_2Cl_2, supporting electrolyte 0.10 M *n*-Bu_4NPF_6, scan rate 100 mV s^{-1}. (b) UV–vis absorption and *PL* of HQTZ in DMSO.

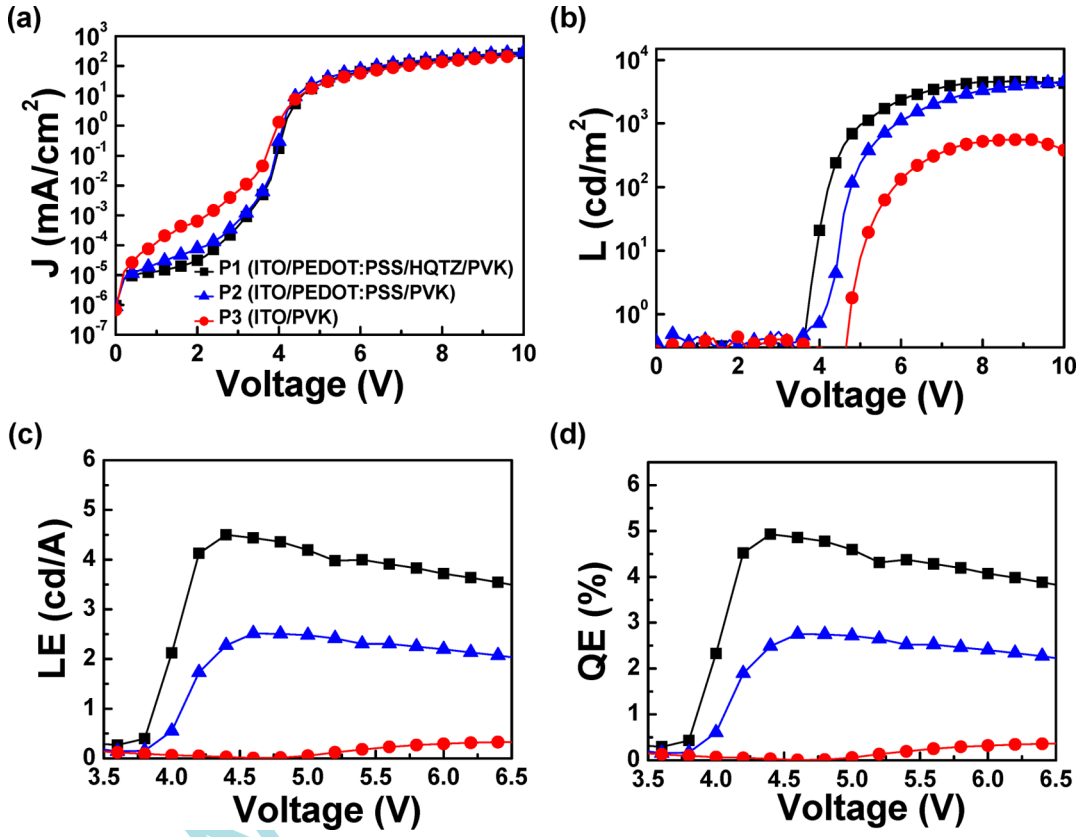

Figure 3. (a) *J*–*V*, (b) *L*–*V*, (c) *LE*–*V*, and (d) *QE*–*V* characteristics of device **P1** (with 20 nm HQTZ), **P2**, and **P3**.

Table 1. Performance of Deep-Blue Fluorescent PLEDs with Different HILs at the Maximum *LE* and *QE*

device	HILs	V_{on}[a] (V)	voltage (V)	*J* (mA/cm^2)	*L* (cd/m^2)	LE_{max} [LE_{avg}[a]] (cd/A)	QE_{max} [QE_{avg}][a] (%)	CIE
P1	PEDOT:PSS/HQTZ(10 nm)/PVK	3.9	5.8	31.8	1103.5	3.47 [2.33]	3.79 [2.55]	(0.16, 0.08)
P1	PEDOT:PSS/HQTZ(20 nm)/PVK	3.7	4.4	5.3	238.6	4.50 [3.52]	4.93 [3.85]	(0.16, 0.09)
P1	PEDOT:PSS/HQTZ(30 nm)/PVK	3.8	5.0	26.5	1028.3	3.88 [2.76]	4.26 [3.07]	(0.16, 0.09)
P2	PEDOT:PSS/PVK	4.1	4.6	14.2	356.4	2.51 [1.79]	2.75 [1.96]	(0.16, 0.08)
P3	PVK	4.7	6.6	79.2	261.3	0.33 [0.21]	0.37 [0.23]	(0.17, 0.10)
P4	HQTZ(20 nm)/PVK	4.3	5.4	16.5	457.1	2.77 [1.87]	3.04 [2.05]	(0.16, 0.11)

[a]V_{on}, turn-on voltage corresponding to 1 cd/m^2; LE_{max}, the maximum luminous efficiency; QE_{max}, the maximum quantum efficiency; LE_{avg}, the average maximum luminous efficiency; QE_{avg}, the average maximum quantum efficiency.

and *QE* of 4.93% are obtained, which are enhanced by 80% compared with those of the conventional device **P2** with the typical ITO/PEDOT:PSS/PVK anode. Moreover, device **P1** with a 20 nm-thick HQTZ layer exhibits a lower turn-on voltage of 3.7 V and CIE coordinates of (0.16, 0.09), which is similar to CIE (0.16, 0.08) of device **P2** and very close to

DOI: 10.1021/acsami.5b06068
ACS Appl. Mater. Interfaces 2015, 7, 26405–26413

Table 2. Performance of Deep-Blue Fluorescent PLEDs with Different HILs at the Current Density of around 35 mA/cm^2

device	HILs	voltage (V)	J (mA/cm^2)	L (cd/m^2)	LE [LE_{avg}][a] (cd/A)	QE [QE_{avg}][a] (%)
P1	PEDOT:PSS/HQTZ(10 nm)/PVK	5.8	31.8	1103.5	3.47 [2.25]	3.79 [2.46]
P1	PEDOT:PSS/HQTZ(20 nm)/PVK	5.4	35.6	1409.8	3.96 [3.32]	4.30 [3.63]
P1	PEDOT:PSS/HQTZ(30 nm)/PVK	5.4	36.3	1343.2	3.70 [2.68]	4.06 [3.04]
P2	PEDOT:PSS/PVK	5.0	32.5	802.7	2.47 [1.61]	2.71 [1.77]
P3	PVK	5.8	35.5	60.4	0.17 [0.13]	0.18 [0.14]
P4	HQTZ(20 nm)/PVK	5.8	33.8	868.7	2.57 [1.72]	2.82 [1.89]

[a] LE_{avg}, the average luminous efficiency around 35 mA/cm^2; QE_{avg}, the average quantum efficiency around 35 mA/cm^2.

NTSC standard blue light with CIE coordinates of (0.14, 0.08). The big influence of a cascade HIL structure can also be demonstrated from the lower efficiency and higher turn-on voltage of **P3** device with the single PVK layer as HIL. The results indicate that none of PEDOT:PSS, HQTZ and PVK layers can be omitted to form cascade hole injection for obtaining the highly efficient deep-blue fluorescent PLEDs. The detailed device parameters with the highest efficiency are summarized in Table 1. For illustrating a real improvement in device performance, the statistical data of maximum *LE* and *QE* of **P1** (with 20 nm HQTZ), **P2**, **P3**, and **P4** are shown in Figure S7. The error bars denote the 25th and 75th percentile values, composed of 23, 25, 17, and 18 separate devices for each type prepared at the same condition. The values of the average maximum *LE* and *QE* are 3.52 cd/A, 1.79 cd/A, 0.21 cd/A, 1.87 cd/A, and 3.85%, 1.96%, 0.23%, 2.05%, respectively, for **P1** (with 20 nm HQTZ), **P2**, **P3**, and **P4**. From these data, it is clear that the device efficiency is highly improved by using HQTZ as the intermediate HIL. In addition, by comparing **P2** and **P4** *J*−*V*, *L*−*V*, *LE*−*V*, and *QE*−*V* curves (Figure S8), we find that HQTZ also shows comparable hole injection property as that of PEDOT:PSS. Since the highly acidic aqueous solution of PEDOT:PSS can gradually corrode ITO anode and eventually degrade device performance and long-term stability,[31] it is promising to use HQTZ as HIL in PLEDs or organic photovoltaic cells in the future. The performance of deep-blue fluorescent PLEDs with different HILs at the operating current density of around 35 mA/cm^2 is shown in Table 2. The *LE* and *QE* of device with PEDOT:PSS/HQTZ(20 nm)/PVK HILs are 3.96 cd/A and 4.30%, respectively, which are much higher than those of devices with PVK or PEDOT:PSS/PVK.

We emphasize that it is quite important to find the optimum HQTZ thickness for highly efficient deep-blue fluorescent PLEDs. Figure S9 presents the *LE*−*L* and *QE*−*L* characteristics of **P1** device with different thickness HQTZ layer. Optimized device with 20 nm-thick HQTZ exhibited a relatively higher efficiency than that of device with 10 nm-thick or 30 nm-thick HQTZ layer. The thinner HQTZ layers did not bring the best results more likely due to the poor electron-blocking ability, which allowed the electrons to tunnel through,[32] while the thicker HQTZ layers may increase the contact resistance.[31] For identifying the electron-blocking capability, the HQTZ layer was introduced between the PSF and poly(*p*-phenylenevinlene) (P-PPV) layers (ITO/PSF/HQTZ/P-PPV/CsF/Al). The green emission is dominant for this device (ITO/PSF/HQTZ/P-PPV/CsF/Al), compared with the P-PPV-only device (ITO/PEDOT:PSS/P-PPV/CsF/Al), as shown in Figure 4. In contrast, a device with the reverse structure of ITO/P-PPV/HQTZ/PSF/CsF/Al shows the blue emission dominantly, although there is a small widening and red-shift emission compared with the pure PSF device (ITO/PEDOT:PSS/PSF/CsF/Al). The results suggest that the

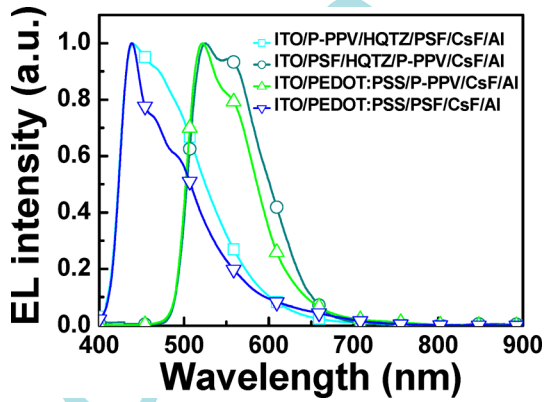

Figure 4. *EL* spectra of devices with the structures of ITO/P-PPV/HQTZ/PSF/CsF/Al, ITO/PSF/HQTZ/P-PPV/CsF/Al, ITO/PEDOT:PSS/P-PPV/CsF/Al, and ITO/PEDOT:PSS/PSF/CsF/Al.

HQTZ layer can effectively block the electron transport from the PSF to the anode, and the recombination between the injected holes and electrons primarily occurs within the PSF layer for **P1** device.

Figure 5, panel a shows the *EL* spectra of device **P1** with 20 nm HQTZ, **P2**, **P3**, and **P4** at 35 mA/cm^2, respectively. The emission peaks at ∼440 nm for each device, coming from the original blue emission of PSF regardless of the type of HILs.[14] However, slightly wide *EL* spectra were found when PEDOT:PSS is not introduced for **P3** and **P4** devices, which may originate from the exciplex formed between PVK and PSF due to the large hole-injection barriers existed in HILs. The better CIE results for devices with HQTZ indicate that the insertion of HQTZ layer is beneficial to make the formed excitons to be limited in the PSF emitter emission zone. The optical transmittance spectra of ITO/PEDOT:PSS/HQTZ(20 nm)/PVK, ITO/PEDOT:PSS/PVK and ITO/HQTZ(20 nm)/PVK are shown in Figure 5, panel b. There is no significant change in the transparence of ITO/PEDOT:PSS/HQTZ(20 nm)/PVK and ITO/PEDOT:PSS/PVK films, illuminating HQTZ layer has hardly any detrimental effect on the light out-coupling of devices. However, a higher transparence from 380−480 nm was detected for ITO/HQTZ(20 nm)/PVK film compared to ITO/PEDOT:PSS/PVK film, which is advantageous to improve blue-light emission for **P4** device in comparison with **P2** device. Figure 5, panel c shows the *PL* spectra of two different films of PEDOT:PSS/HQTZ(20 nm)/PVK/PSF(10 nm) and PEDOT:PSS/PVK/PSF(10 nm) processed on quartz. The *PL* intensity of quartz/PEDOT:PSS/HQTZ(20 nm)/PVK/PSF(10 nm) shows much higher *PL* intensity compared to that of quartz/PEDOT:PSS/PVK/PSF(10 nm), which is consistent to its highest device *EL* efficiency. The HQTZ interlayer prevents significant quenching of radiative excitons between the active layer and the HQTZ

DOI: 10.1021/acsami.5b06068
ACS Appl. Mater. Interfaces 2015, 7, 26405−26413

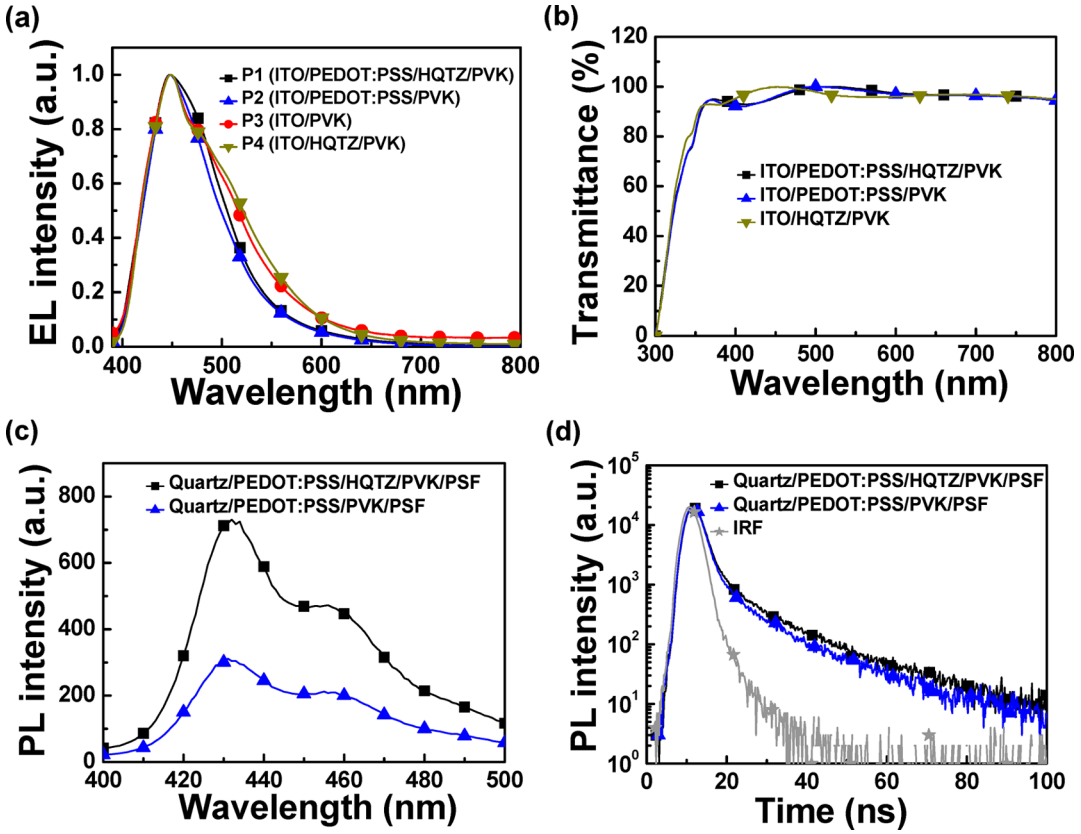

Figure 5. (a) Normalized *EL* spectra of **P1** (with 20 nm HQTZ), **P2**, **P3**, and **P4** devices. (b) Transmittance spectra of ITO/PEDOT:PSS/HQTZ(20 nm)/PVK, ITO/PEDOT:PSS/PVK, and ITO/HQTZ(20 nm)/PVK. (c) *PL* spectra of PSF (10 nm) films processed on quartz/PEDOT:PSS/HQTZ(20 nm)/PVK and quartz/PEDOT:PSS/PVK. (d) Time-resolved transient *PL* spectra of quartz/PEDOT:PSS/HQTZ(20 nm)/PVK/PSF(10 nm) and quartz/PEDOT:PSS/PVK/PSF(10 nm).

layer, thus enhancing the device performance. To investigate the intrinsic reason, the exciton lifetime of PSF was measured, as shown in Figure 5, panel d. The total instrument response function (IRF) for *PL* decay is less than 30 ps, and the time resolution is less than 10 ps. The exciton lifetime at 440 nm for quartz/PEDOT:PSS/HQTZ(20 nm)/PVK/PSF(10 nm) film shows the longer exciton lifetime of 4.576 ns than that of quartz/PEDOT:PSS/PVK/PSF(10 nm) of 3.258 ns. It indicates that exciton quenching becomes smaller after the insertion of HQTZ layer between PEDOT:PSS and PVK. The efficient *PL* intensity enhancement and the increase of exciton emission lifetime at 440 nm imply that PSF singlet excitons can more efficiently come into being for **P1** device.

To further illustrate the internal physics mechanism, the surface work functions of HILs-modified ITO were measured by scanning Kelvin probe force microscopy (SKPFM). The work functions of ITO/PEDOT:PSS/HQTZ(20 nm)/PVK, ITO/PEDOT:PSS/PVK, ITO/HQTZ(20 nm)/PVK, ITO/PVK, and ITO/HQTZ are 5.13 eV, 5.09 eV, 4.85 eV, 4.78 eV, and 4.76 eV, respectively, as shown in Figure 6, panel a. Apparently, the insertion of HQTZ layer can efficiently improve the surface work function of HILs-modified ITO, which is advantageous to facilitate the hole injection from HILs-modified ITO to the deep-blue emitter PSF. Besides, it can be seen that the single HQTZ layer can efficiently enhance the work function of ITO (4.65 eV) to more than 0.11 eV, which is similar to the single PVK layer (0.13 eV). Meanwhile, ultraviolet photoelectron spectroscopy (UPS) measurements were performed with monochromatized HeI radiation at 21.2 eV. The surface work function is defined by the secondary electron cutoff. From the UPS measurements, the work function value of Au/PEDOT:PSS/HQTZ/PVK and Au/PEDOT:PSS/PVK is 4.0 and 3.8 eV, respectively, as shown in Figure 6, panel b. The results are quite similar to the UPS measurements performed on two differently synthesized PEDOT samples with the work function values of 4.0 and 4.4 eV.[33] The work function values of UPS are consistent to those of SKPFM, illustrating that the insertion of HQTZ layer can effectively further lower the barrier of hole injection from HILs-modified ITO to PSF and enhance the device performance. Furthermore, the photovoltaic measurements were also conducted to determine the open-circuit voltage (V_{oc}) value, which is decided by the difference of work function of the electrodes based on metal−insulator−metal model,[34] shown in Figure 6, panel c. The V_{oc} value of **P1** with 20 nm HQTZ, **P2**, and **P3** is 1.88 V, 1.76 V, and 1.72 V, respectively, implying that the barrier height of hole injection decreases when the HQTZ layer is inserted. The photovoltaic results are consistent with those of SKPFM and UPS measurements.

The insertion of HQTZ layer between PEDOT:PSS and PVK not only enhances the hole injection, but also improves the hole transport in HILs. The hole mobility of the HILs was measured by space-charge-limited current (SCLC) model with the equation of $J = (9/8)\ \varepsilon_r\varepsilon_0\mu\ (V^2/d^3)$.[35] The hole mobility was measured by hole-only device with the structures of ITO/MoO_3(10 nm)/PEDOT:PSS(40 nm)/HQTZ(20 nm)/PVK-(35 nm)/PSF(75 nm)/MoO_3(10 nm)/Al and ITO/MoO_3(10 nm)/PEDOT:PSS(40 nm)/PVK(35 nm)/PSF(75 nm)/

DOI: 10.1021/acsami.5b06068
ACS Appl. Mater. Interfaces 2015, 7, 26405−26413

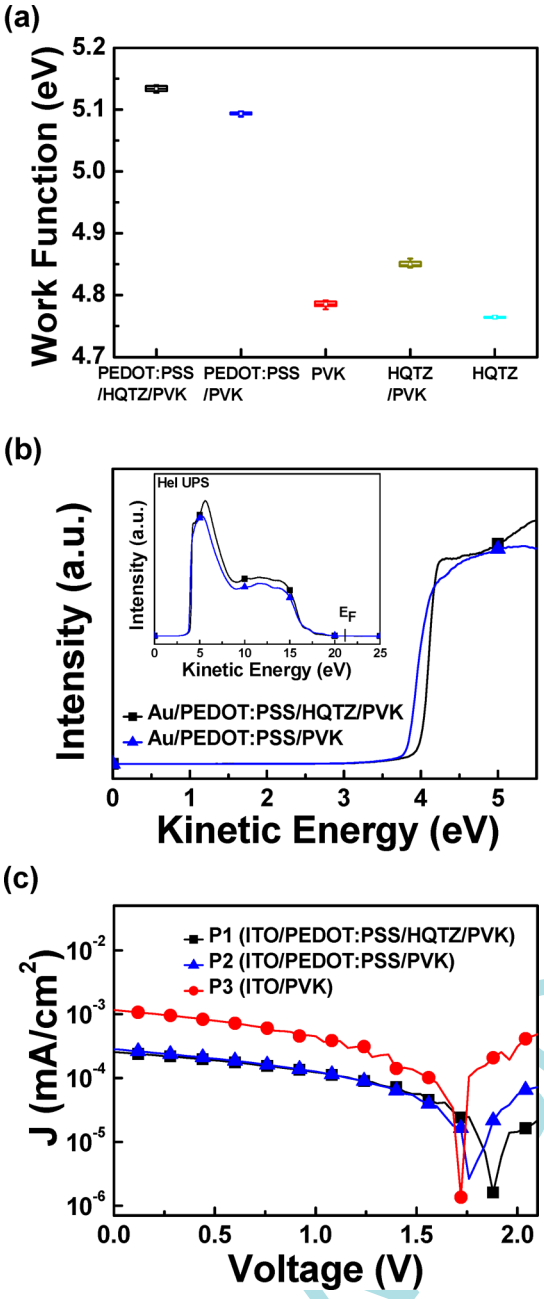

Figure 6. (a) Surface work function of HILs-modified ITO by SKPFM. (b) The secondary electron cutoff of UPS based on Au/PEDOT:PSS/HQTZ/PVK and Au/PEDOT:PSS/PVK; these two types of structures of UPS are shown in the inset of panel b. (c) *J*–*V* characteristics of **P1** with 20 nm HQTZ, **P2**, and **P3** devices under AM 1.5G solar simulator with an intensity of 100 mW/cm^2.

MoO_3(10 nm)/Al. As shown in Figure S10, the hole mobility of the device with HQTZ is about 4.66×10^{-5} cm^2 V^{-1} s^{-1}, which is two-orders higher than that of device without HQTZ (3.99×10^{-7} cm^2 V^{-1} s^{-1}). Thus, it can be seen that the HQTZ layer extraordinarily enhances the hole transport/injection at the same time. For verifying the carrier balance whether or not in device, we also fabricated electron-only device with the structures of ITO/Al(80 nm)/CsF(1 nm)/PEDOT:PSS(40 nm)/HQTZ(20 nm)/PVK(35 nm)/PSF(75 nm)/CsF(1 nm)/Al and ITO/Al(80 nm)/CsF(1 nm)/PEDOT:PSS(40 nm)/PVK(35 nm)/PSF(75 nm)/CsF(1 nm)/Al. The electron mobility of the device with HQTZ is about 6.26×10^{-5} cm^2 V^{-1} s^{-1}, which is a little higher than that of electron-only device without HQTZ (1.47×10^{-5} cm^2 V^{-1} s^{-1}) and comparable to the hole mobility of hole-only device with HQTZ (4.66×10^{-5} cm^2 V^{-1} s^{-1}), indicating that the hole and electron carriers are well balanced with the insertion of HQTZ layer. The simultaneous improvements of the hole injection/transport and the hole/electron balance ultimately lead to the enhancement of **P1** device performance. These are consistent to the data in Table 2. To further study the carrier mobility of pure HQTZ material, the hole-only device with the structure of ITO/MoO_3(10 nm)/HQTZ(80 nm)/MoO_3(10 nm)/Al and the electron-only device with the structure of ITO/Al(80 nm)/CsF(1 nm)/HQTZ(80 nm)/CsF(1 nm)/Al were also prepared (see Figure S11). The hole and electron mobilities of HQTZ are 5.95×10^{-5} cm^2 V^{-1} s^{-1} and 1.91×10^{-6} cm^2 V^{-1} s^{-1}, respectively. The bipolar transport observed through SCLC suggests that HQTZ is an efficient and versatile material for various applications in PLEDs.

Low surface roughness is very important to obtain an even hole injection with unlocalized electric field and will delay the deterioration of organic materials and devices.[36] Figure 7,

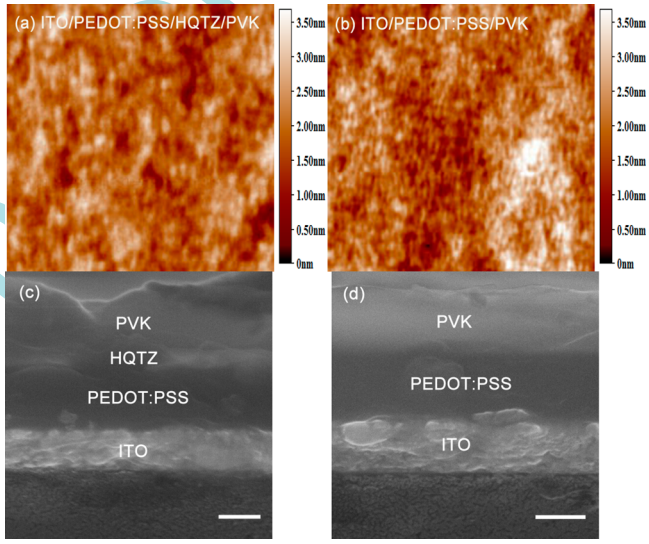

Figure 7. AFM images of (a) ITO/PEDOT:PSS/HQTZ(20 nm)/PVK and (b) ITO/PEDOT:PSS/PVK. The SEM cross-section images of (c) ITO/PEDOT:PSS/HQTZ/PVK and (d) ITO/PEDOT:PSS/PVK. (AFM image dimensions = 5 μm × 5 μm and SEM bar = 200 nm).

panels a and b show the AFM images of ITO/PEDOT:PSS/HQTZ(20 nm)/PVK and ITO/PEDOT:PSS/PVK films. The surface root−mean−square (RMS) roughness with the insertion of 20 nm-thick HQTZ layer is 0.51 nm, whereas the RMS roughness is increased to 0.56 nm without the HQTZ layer. This indicates that there exists perfect interface contact when HQTZ is introduced between PEDOT:PSS and PVK. The well-distributed electric field for **P1** device may inhibit composite excitons to dissociate into positive and negative charges, leading to the enhancement of **P1** device performance. Interface intermixing is another factor that one may consider to influence the device performance. Figure 7, panels c and d show the SEM cross-section images of ITO/PEDOT:PSS/HQTZ/PVK and ITO/PEDOT:PSS/PVK films. The intermixing at the PEDOT:PSS/HQTZ or HQTZ/PVK interface is minimal, suggesting that HQTZ is suitable and feasible to be used in

DOI: 10.1021/acsami.5b06068
ACS Appl. Mater. Interfaces 2015, 7, 26405−26413

multilayer HILs. We owe the reason to the worse solubility of top PVK layer in dimethyl sulfoxide, as shown in Figure S12. All results illustrate that HQTZ can be a promising candidate of hole interfacial materials for deep-blue fluorescent PLEDs.

CONCLUSION

In this paper, a novel material HQTZ was developed and introduced between PEDOT:PSS and PVK in deep-blue fluorescent PLEDs as an intermediate HIL. The maximum *LE* and *QE* of device adopting the HQTZ layer are improved by 80% compared to conventional device with PEDOT:PSS/PVK. *PL* and time-resolved transient *PL* spectra reveal that HQTZ layer can effectively prevent the radiative excitons quenching in conjunction with the good electron blocking ability. SKPFM, UPS, and photovoltaic measurements show that HQTZ layer can further increase the surface work function and reduce the barrier of hole injection in PLEDs. Furthermore, the hole mobility is enormously enhanced, and the charge carriers are efficiently balanced, which is also favorable to improve the deep-blue device performance. Moreover, HQTZ material can form good contact with PEDOT:PSS and PVK, which is beneficial to improve the device stability. The results illustrate that HQTZ as a promising candidate of hole interfacial materials has a wonderful application prospect in deep-blue fluorescent PLEDs.

ASSOCIATED CONTENT

Supporting Information

The Supporting Information is available free of charge on the ACS Publications website at DOI: 10.1021/acsami.5b06068.

^{1}H NMR; ^{13}C NMR; ESI mass spectrometer; MALDI-TOF; energy level diagram; thermogravimetric analysis; box charts of device efficiencies; details of *J*−*V*, *L*−*V*, *LE*−*V*, and *QE*−*V* curves of **P2** and **P4** devices; *LE*−*L* and *QE*−*L* characteristics of device **P1** with different HQTZ thickness; SCLC measurement; thin-film photographs (PDF)

AUTHOR INFORMATION

Corresponding Authors

*E-mail: thlt@jnu.edu.cn.
*E-mail: celiy@scut.edu.cn.

Author Contributions

L.X. and Y.X. contributed equally to this work.

Notes

The authors declare no competing financial interest.

ACKNOWLEDGMENTS

The authors are grateful to the NSFC Project (11204106, 61274062, 21402054, and 21174042), the Open Fund of the State Key Laboratory of Luminescent Materials and Devices (South China University of Technology 2012-skllmd-10), and the Fundamental Research Funds for the Central Universities for financial support.

REFERENCES

(1) Park, S.-I.; Xiong, Y.; Kim, R.-H.; Elvikis, P.; Meitl, M.; Kim, D.-H.; Wu, J.; Yoon, J.; Yu, C.-J.; Liu, Z.; Huang, Y.; Hwang, K.-c.; Ferreira, P.; Li, X.; Choquette, K.; Rogers, J. A. Printed Assemblies of Inorganic Light-Emitting Diodes for Deformable and Semitransparent Displays. *Science* **2009**, *325*, 977−981.

(2) Nguyen, T. D.; Ehrenfreund, E.; Vardeny, Z. V. Spin-Polarized Light-Emitting Diode Based on an Organic Bipolar Spin Valve. *Science* **2012**, *337*, 204−209.

(3) Niikura, H.; Legare, F.; Hasbani, R.; Ivanov, M. Y.; Villeneuve, D. M.; Corkum, P. B. Probing Molecular Dynamics with Attosecond Resolution Using Correlated Wave Packet Pairs. *Nature* **2003**, *421*, 826−829.

(4) Muller, C. D.; Falcou, A.; Reckefuss, N.; Rojahn, M.; Wiederhirn, V.; Rudati, P.; Frohne, H.; Nuyken, O.; Becker, H.; Meerholz, K. Multi-Colour Organic Light-Emitting Displays by Solution Processing. *Nature* **2003**, *421*, 829−833.

(5) Yang, C.; Song, H.-S.; Liu, D.-B. Pure Blue Light-Emitting Fluorene-Based Conjugated Polymer with Excellent Thermal, Photophysical, and Electroluminescent Properties. *J. Mater. Sci.* **2013**, *48*, 6719−6727.

(6) Wang, L.; Jiang, Y.; Luo, J.; Zhou, Y.; Zhou, J. H.; Wang, J.; Pei, J.; Cao, Y. Highly Efficient and Color-Stable Deep-Blue Organic Light-Emitting Diodes Based on a Solution-Processible Dendrimer. *Adv. Mater.* **2009**, *21*, 4854−4858.

(7) Kang, D. M.; Kang, J.-W.; Park, J. W.; Jung, S. O.; Lee, S.-H.; Park, H.-D.; Kim, Y.-H.; Shin, S. C.; Kim, J.-J.; Kwon, S.-K. Iridium Complexes with Cyclometalated 2-Cycloalkenyl-Pyridine Ligands as Highly Efficient Emitters for Organic Light-Emitting Diodes. *Adv. Mater.* **2008**, *20*, 2003−2007.

(8) Wang, E.; Li, C.; Mo, Y.; Zhang, Y.; Ma, G.; Shi, W.; Peng, J.; Yang, W.; Cao, Y. Poly(3,6-silafluorene-co-2,7-fluorene)-Based High-Efficiency and Color-Pure Blue Light-Emitting Polymers with Extremely Narrow Band-Width and High Spectral Stability. *J. Mater. Chem.* **2006**, *16*, 4133−4140.

(9) Huang, F.; Zhang, Y.; Liu, M. S.; Cheng, Y. J.; Jen, A. K. Y. High-Efficiency and Color Stable Blue-Light-Emitting Polymers and Devices. *Adv. Funct. Mater.* **2007**, *17*, 3808−3815.

(10) Xing, X.; Zhang, L.; Liu, R.; Li, S.; Qu, B.; Chen, Z.; Sun, W.; Xiao, L.; Gong, Q. A Deep-Blue Emitter with Electron Transporting Property to Improve Charge Balance for Organic Light-Emitting Device. *ACS Appl. Mater. Interfaces* **2012**, *4*, 2877−2880.

(11) Huang, C.-W.; Tsai, C.-L.; Liu, C.-Y.; Jen, T.-H.; Yang, N.-J.; Chen, S.-A. Design of Deep Blue Electroluminescent Spiro-Polyfluorenes with High Efficiency by Facilitating the Injection of Charge Carriers through Incorporation of Multiple Charge Transport Moieties. *Macromolecules* **2012**, *45*, 1281−1287.

(12) Cao, Y.; Yu, G.; Parker, I. D.; Heeger, A. J. Ultrathin Layer Alkaline Earth Metals as Stable Electron-Injecting Electrodes for Polymer Light Emitting Diodes. *J. Appl. Phys.* **2000**, *88*, 3618−3623.

(13) Stolz, S.; Scherer, M.; Mankel, E.; Lovrincic, R.; Schinke, J.; Kowalsky, W.; Jaegermann, W.; Lemmer, U.; Mechau, N.; Hernandez-Sosa, G. Investigation of Solution-Processed Ultrathin Electron Injection Layers for Organic Light-Emitting Diodes. *ACS Appl. Mater. Interfaces* **2014**, *6*, 6616−6622.

(14) Wang, J.; Zhang, C. Q.; Zhong, C. M.; Hu, S. J.; Chang, X. Y.; Mo, Y. Q.; Chen, X.; Wu, H. B. Highly Efficient and Stable Deep Blue Light Emitting Poly(9,9-dialkoxyphenyl- 2,7-silafluorene): Synthesis and Electroluminescent Properties. *Macromolecules* **2011**, *44*, 17−19.

(15) Ho, C. L.; Wong, W. Y.; Gao, Z. Q.; Chen, C. H.; Cheah, K. W.; Yao, B.; Xie, Z. Y.; Wang, Q.; Ma, D. G.; Wang, L. X.; Yu, X. M.; Kwok, H. S.; Lin, Z. Y. Red-Light-Emitting Iridium Complexes with Hole-Transporting 9-Arylcarbazole Moieties for Electrophosphorescence Efficiency/Color Purity Trade-off Optimization. *Adv. Funct. Mater.* **2008**, *18*, 319−331.

(16) Kulkarni, A. P.; Gifford, A. P.; Tonzola, C. J.; Jenekhe, S. A. Efficient Blue Organic Light-Emitting Diodes Based on an Oligoquinoline. *Appl. Phys. Lett.* **2005**, *86*, 061106.

(17) Nicolai, H. T.; Wetzelaer, G. A. H.; Kuik, M.; Kronemeijer, A. J.; de Boer, B.; Blom, P. W. M. Space-Charge-Limited Hole Current in Poly(9,9-dioctylfluorene) Diodes. *Appl. Phys. Lett.* **2010**, *96*, 172107.

(18) Zhou, M.; Chua, L.-L.; Png, R.-Q.; Yong, C.-K.; Sivaramakrishnan, S.; Chia, P.-J.; Wee, A.; Friend, R.; Ho, P. Role of δ-Hole-Doped Interfaces at Ohmic Contacts to Organic Semiconductors. *Phys. Rev. Lett.* **2009**, *103*, 036601.

DOI: 10.1021/acsami.5b06068
ACS Appl. Mater. Interfaces 2015, 7, 26405−26413

(19) Helander, M. G.; Wang, Z. B.; Qiu, J.; Greiner, M. T.; Puzzo, D. P.; Liu, Z. W.; Lu, Z. H. Chlorinated Indium Tin Oxide Electrodes with High Work Function for Organic Device Compatibility. *Science* **2011**, *332*, 944−947.
(20) Yang, X.; Xu, X.; Zhou, G. Recent Advances of the Emitters for High Performance Deep-Blue Organic Light-Emitting Diodes. *J. Mater. Chem. C* **2015**, *3*, 913−944.
(21) Fink, R.; Frenz, C.; Thelakkat, M.; Schmidt, H.-W. Synthesis and Characterization of Aromatic Poly(1,3,5-triazine−ether)s for Electroluminescent Devices. *Macromolecules* **1997**, *30*, 8177−8181.
(22) Klenkler, R. A.; Aziz, H.; Tran, A.; Popovic, Z. D.; Xu, G. High Electron Mobility Triazine for Lower Driving Voltage and Higher Efficiency Organic Light Emitting Devices. *Org. Electron.* **2008**, *9*, 285−290.
(23) Kang, J.-W.; Lee, D.-S.; Park, H.-D.; Park, Y.-S.; Kim, J. W.; Jeong, W.-I.; Yoo, K.-M.; Go, K.; Kim, S.-H.; Kim, J.-J. Silane- and Triazine-Containing Hole and Exciton Blocking Material for High-Efficiency Phosphorescent Organic Light Emitting Diodes. *J. Mater. Chem.* **2007**, *17*, 3714−3719.
(24) Do, K.; Choi, H.; Lim, K.; Jo, H.; Cho, J. W.; Nazeeruddin, M. K.; Ko, J. Star-Shaped Hole Transporting Materials with a Triazine Unit for Efficient Perovskite Solar Cells. *Chem. Commun.* **2014**, *50*, 10971−10974.
(25) Liu, X. K.; Zheng, C. J.; Xiao, J.; Ye, J.; Liu, C. L.; Wang, S. D.; Zhao, W. M.; Zhang, X. H. Novel Bipolar Host Materials Based on 1,3,5-Triazine Derivatives for Highly Efficient Phosphorescent OLEDs with Extremely Low Efficiency Roll-off. *Phys. Chem. Chem. Phys.* **2012**, *14*, 14255−14261.
(26) Zou, Y.; Zou, J.; Ye, T.; Li, H.; Yang, C.; Wu, H.; Ma, D.; Qin, J.; Cao, Y. Unexpected Propeller-Like Hexakis(fluoren-2-yl)benzene Cores for Six-Arm Star-Shaped Oligofluorenes: Highly Efficient Deep-Blue Fluorescent Emitters and Good Hole-Transporting Materials. *Adv. Funct. Mater.* **2013**, *23*, 1781−1788.
(27) Gong, X.; Wang, S.; Moses, D.; Bazan, G. C.; Heeger, A. J. Multilayer Polymer Light-Emitting Diodes: White-Light Emission with High Efficiency. *Adv. Mater.* **2005**, *17*, 2053−2058.
(28) Giovanella, U.; Botta, C.; Galeotti, F.; Vercelli, B.; Battiato, S.; Pasini, M. Perfluorinated Polymer with Unexpectedly Efficient Deep Blue Electroluminescence for Full-Colour OLED Displays and Light Therapy Applications. *J. Mater. Chem. C* **2013**, *1*, 5322−5329.
(29) Wang, E.; Li, C.; Mo, Y.; Zhang, Y.; Ma, G.; Shi, W.; Peng, J.; Yang, W.; Cao, Y. Poly(3,6-silafluorene-co-2,7-fluorene)-Based High-Efficiency and Color-Pure Blue Light-Emitting Polymers with Extremely Narrow Band-Width and High Spectral Stability. *J. Mater. Chem.* **2006**, *16*, 4133−4140.
(30) Bathfield, M.; Daviot, D.; D'Agosto, F.; Spitz, R.; Ladavière, C.; Charreyre, M.-T.; Delair, T. Synthesis of Lipid-α-End-Functionalized Chains by RAFT Polymerization. Stabilization of Lipid/Polymer Particle Assemblies. *Macromolecules* **2008**, *41*, 8346−8353.
(31) Lee, B. R.; Kim, J. W.; Kang, D.; Lee, D. W.; Ko, S. J.; Lee, H. J.; Lee, C. L.; Kim, J. Y.; Shin, H. S.; Song, M. H. Highly Efficient Polymer Light-Emitting Diodes Using Graphene Oxide as a Hole Transport Layer. *ACS Nano* **2012**, *6*, 2984−2991.
(32) Gupta, D.; Katiyar, M. Deepak, Various Approaches to White Organic Light Emitting Diodes and Their Recent Advancements. *Opt. Mater.* **2006**, *28*, 295−301.
(33) Gross, M.; Muller, D. C.; Nothofer, H. G.; Scherf, U.; Neher, D.; Brauchle, C.; Meerholz, K. Improving the Performance of Doped Pi-Conjugated Polymers for Use in Organic Light-Emitting Diodes. *Nature* **2000**, *405*, 661−665.
(34) Chu, Y. L.; Cheng, C. C.; Yen, Y. C.; Chang, F. C. A New Supramolecular Hole Injection/Transport Material on Conducting Polymer for Application in Light-Emitting Diodes. *Adv. Mater.* **2012**, *24*, 1894−1898.
(35) Ogawa, T.; Cho, D. C.; Kaneko, K.; Mori, T.; Mizutani, T. Numerical Analysis of the Carrier Behavior of Organic Light-Emitting Diode: Comparing a Hopping Conduction Model with a SCLC Model. *Thin Solid Films* **2003**, *438-439*, 171−176.
(36) Hou, L.; Liu, P.; Li, Y.; Wu, C. Enhanced Performance in Organic Light-Emitting Diodes by Sputtering TiO2 Ultra-Thin Film as the Hole Buffer Layer. *Thin Solid Films* **2009**, *517*, 4926−4929.

DOI: 10.1021/acsami.5b06068
ACS Appl. Mater. Interfaces 2015, 7, 26405−26413